AGU PUBLICATIONS

Water Resources Research

RESEARCH ARTICLE
10.1002/2016WR019655

Key Points:
- Ar, Kr, and Xe isotope ratios were measured throughout a 110 m unsaturated zone
- Steady state isotopic fractionation of heavy noble gases is strongly dependent on depth
- Dissolved Ar, Kr, and Xe isotopes in paleogroundwater may enable past water table depth estimation

Supporting Information:
- Supporting Information S1
- Data Set S1

Correspondence to:
A. M. Seltzer,
aseltzer@ucsd.edu

Citation:
Seltzer, A. M., J. P. Severinghaus, B. J. Andraski, and D. A. Stonestrom (2017), Steady state fractionation of heavy noble gas isotopes in a deep unsaturated zone, *Water Resour. Res.*, *53*, 2716–2732, doi:10.1002/2016WR019655.

Received 16 AUG 2016
Accepted 26 FEB 2017
Accepted article online 2 MAR 2017
Published online 6 APR 2017

Steady state fractionation of heavy noble gas isotopes in a deep unsaturated zone

Alan M. Seltzer[1], Jeffrey P. Severinghaus[1], Brian J. Andraski[2], and David A. Stonestrom[3]

[1]Scripps Institution of Oceanography, University of California, San Diego, California, USA, [2]U.S. Geological Survey, Carson City, Nevada, USA, [3]U.S. Geological Survey, Menlo Park, California, USA

Abstract To explore steady state fractionation processes in the unsaturated zone (UZ), we measured argon, krypton, and xenon isotope ratios throughout a ~110 m deep UZ at the United States Geological Survey (USGS) Amargosa Desert Research Site (ADRS) in Nevada, USA. Prior work has suggested that gravitational settling should create a nearly linear increase in heavy-to-light isotope ratios toward the bottom of stagnant air columns in porous media. Our high-precision measurements revealed a binary mixture between (1) expected steady state isotopic compositions and (2) unfractionated atmospheric air. We hypothesize that the presence of an unsealed pipe connecting the surface to the water table allowed for direct inflow of surface air in response to extensive UZ gas sampling prior to our first (2015) measurements. Observed isotopic resettling in deep UZ samples collected a year later, after sealing the pipe, supports this interpretation. Data and modeling each suggest that the strong influence of gravitational settling and weaker influences of thermal diffusion and fluxes of CO_2 and water vapor accurately describe steady state isotopic fractionation of argon, krypton, and xenon within the UZ. The data confirm that heavy noble gas isotopes are sensitive indicators of UZ depth. Based on this finding, we outline a potential inverse approach to quantify past water table depths from noble gas isotope measurements in paleogroundwater, after accounting for fractionation during dissolution of UZ air and bubbles.

1. Introduction

Noble gases in nature have widespread applications as conservative tracers of physical processes. Because of their inertness in chemical and biological processes, and approximately constant atmospheric abundance over long time scales [*Phillips*, 1981], noble gases and their isotopes in groundwater [*Mazor*, 1972; *Stute et al*., 1995], lakes [*Kipfer et al*., 2002; *Tomonaga et al*., 2012], seawater [*Hamme and Severinghaus*, 2007; *Stanley and Jenkins*, 2013], polar ice bubbles [*Severinghaus et al*., 1998], sand [*Severinghaus et al*. 1996], and firn [*Severinghaus and Battle*, 2006; *Kawamura et al*., 2013], among other substrates, have been used as quantitative tools to estimate physical properties and explore processes in natural systems. This study evaluates heavy noble gas isotopes in a deep unsaturated zone (UZ) as possible indicators of depth. Although noble gas isotopes in the UZ have been measured in several recent studies [*Freundt et al*., 2013; *Guillon et al*., 2016], this study is the first to our knowledge to resolve UZ fractionation at a precision of $<0.01‰$ per isotopic mass difference (amu). We compare depth profiles of argon, xenon, and krypton isotope ratios measured above a ~110 m deep water table to profiles predicted by a theoretical fractionation model based on *Severinghaus et al*. [1996].

This study is motivated by the potential for future measurements of dissolved noble gas isotopes in paleogroundwater to quantify water table depth at the time of recharge. Because dissolved gases in groundwater are inherited from the UZ, quantitative information about past water table depth may be retained in paleogroundwater sequestered from the atmosphere since the time of recharge. Paleotemperature estimation from dissolved bulk Ne, Ar, Kr, and Xe concentrations, a common application of atmospheric noble gases in the subsurface, assumes that soil gas of atmospheric composition dissolves into groundwater [*Stute and Schlosser*, 1993]. Noble gas temperature (NGT) models neglect fractionation in the UZ between the free atmosphere and water table because its thickness (i.e., water table depth at the time of recharge) is usually unknown. NGTs are typically assumed to represent mean annual surface temperature (MAST) for water tables around 10 m (in midlatitudes), because the amplitude of the seasonal temperature cycle is nearly

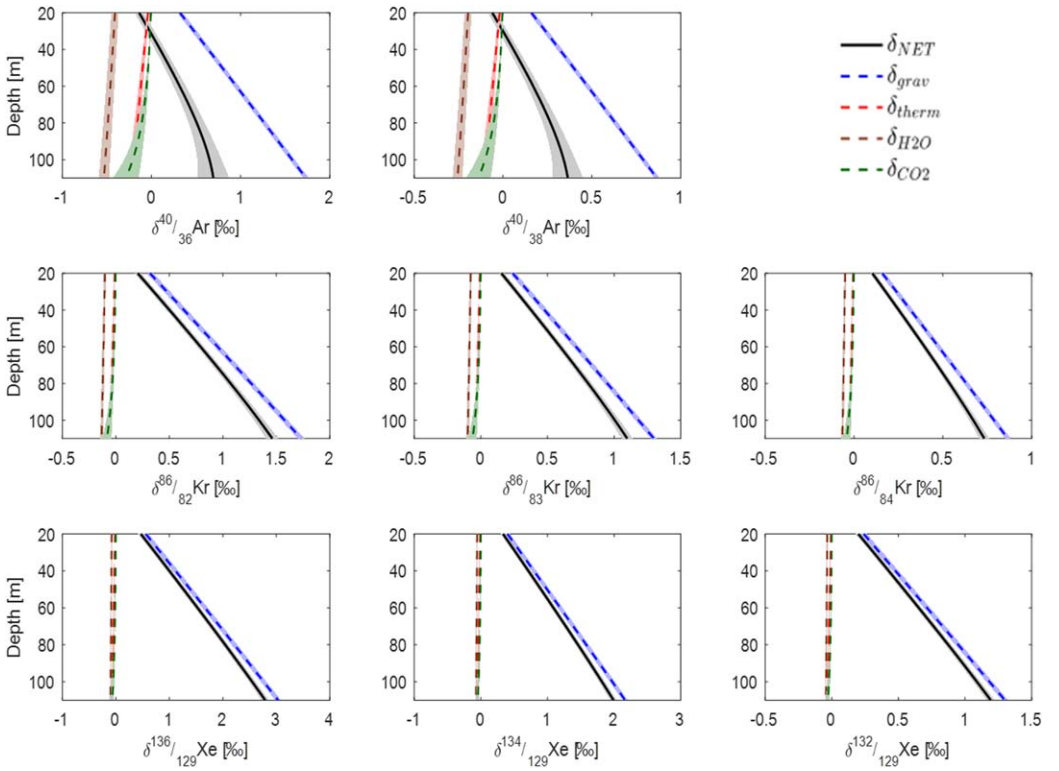

Figure 1. Modeled steady state isotopic fractionation (net and individual components) at ADRS. Inputs to the model include the mean values and uncertainties of 8 years of micrometeorological data from ADRS [*Johnson et al*., 2002, 2007], measurement-based CO_2 profiles (supporting information Figure S4) [*Walvoord et al*., 2005], and the assumption of water vapor saturation below 20 m. Shaded regions indicate 2σ uncertainties of each fractionation component from 1000 Monte Carlo simulations.

completely damped in soil below this depth [*Aeschbach-Hertig and Solomon*, 2013; *Stute and Schlosser*, 1993]. However, the lack of past water table depth information introduces a potential bias in the conversion of NGTs to past MAST due to the contribution of geothermal heat. For example, NGTs of paleogroundwater that equilibrated at water tables much deeper than 10 m would be warmer than MAST at the time of recharge, because temperature generally increases with depth in the shallow lithosphere. With knowledge of past water table depth, measurement of current geothermal gradient, and the assumption that geothermal gradients in the subsurface are constant on time scales of at least 10 kyr, this bias could be removed from NGT-based MAST reconstructions as follows:

$$\mathrm{MAST} = \mathrm{NGT} - \Gamma(z_{WT} - z_{MAST}) \quad (1)$$

where Γ is the mean geothermal gradient (°C m^{-1}), z_{WT} is mean water table depth (m) at the time of recharge, and z_{MAST} is the depth (m) at which MAST applies. The opportunities to implement this paleotemperature correction and to gain quantitative past hydroclimatic constraints from reconstructions of past water table depths are both key motivations of our study to quantify the actual steady state noble gas isotopic fractionation in the UZ.

We begin by presenting a model for steady state isotopic profiles in UZ air (Figure 1). We then test this model in a deep UZ at the US Geological Survey (USGS) Amargosa Desert Research Site (ADRS) near Beatty, Nevada, USA. The ADRS is located adjacent to a closed, low-level radioactive waste (LLRW) disposal site and presents a unique challenge due to its perturbed thermal structure [*Mayers et al*., 2005], elevated CO_2 [*Stonestrom et al*., 2004] and volatile organic compound (VOC) concentrations [*Baker et al*., 2012], and capacity for atmospheric contamination of deep soil air. Finally, we present two inverse model applications for a suite of heavy noble gas isotope measurements: (1) quantifying atmospheric contamination of steady state UZ air at ADRS and (2) estimating past UZ thickness from reconstructed past steady state UZ noble gas isotope ratios (e.g., from dissolved gas measurements in paleogroundwater).

1.1. Isotopic Fractionation in the Unsaturated Zone

Noble gases in the unsaturated zone are effective physical tracers of advection and diffusion in porous media, as confirmed by both field [*Weeks et al*., 1982] and laboratory [*Ding et al*., 2016] studies. In an idealized one-dimensional UZ, atmospheric noble gases diffuse to reach steady state concentrations. The ratio of steady state concentrations of two inert gas species can be described as the sum of three fractionation processes: gravitational settling, thermal diffusion, and diffusion against constant fluxes of other gases (typically water vapor) as suggested by measurements of O_2 and N_2 isotope ratios in a sand dune [*Severinghaus et al*., 1996]. Formally, the idealized steady state ratio of any two gas species (e.g., two noble gas isotopes), δ_{NET}, in a one-dimensional unsaturated zone is given by

$$\delta_{\mathrm{NET}} = \delta_{\mathrm{grav}} + \delta_{\mathrm{therm}} + \delta_{\mathrm{diff}} \tag{2}$$

where δ_{grav}, δ_{therm}, and δ_{diff} are the magnitudes of fractionation due to gravitational settling, thermal diffusion, and diffusion against vertical fluxes. δ_i is defined for any isotope ratio, *i*, as

$$\delta_i = \delta^a/_b X = \left(\frac{\left(\frac{a}{b}\right)_{smp}}{\left(\frac{a}{b}\right)_{atm}} - 1 \right) \times 10^3‰ \tag{3}$$

where *a* and *b*, respectively, are mass numbers of heavy and light isotopes of gas *X*. The fractions $\left(\frac{a}{b}\right)_{smp}$ and $\left(\frac{a}{b}\right)_{atm}$ are concentration ratios measured in sample gas and dry atmospheric air, respectively. We define in more detail the three main components of δ_{NET} throughout this section. Figure 1 shows expected steady state δ_i profiles (section 2.1) for each of the isotope ratios measured in this study.

1.1.1. Gravitational Settling

In a column of gas in hydrostatic balance, total pressure increases exponentially with depth. Individual gas partial pressures are governed by the same balance, such that denser gas species increase in concentration (pressure) more than light species with depth. This enrichment of heavy versus light gas species is known as gravitational settling and has been observed in nature in porous media such as firn [*Craig et al*., 1988] and sand dunes [*Severinghaus et al*., 1996]. Its steady state effect, expressed in delta notation, for any gas ratio, *i*, is given (in ‰) by

$$\delta_{\mathrm{grav}}(i,z) = \left[\exp\left(\frac{\Delta m_i g z}{RT(z)} \right) - 1 \right] \times 10^3‰ \tag{4}$$

where Δm_i is the mass difference in kg mol^{-1} between the heavy and light isotopes in ratio *i*, *g* is gravitational acceleration (9.8 m s^{-2}), *z* is depth in m (with *z* positive downward), *R* is the ideal gas constant (8.314 J K^{-1} mol^{-1}), and *T*(*z*) is mean temperature in K at depth *z*.

1.1.2. Thermal Diffusion

In the presence of a temperature gradient in a column of gas, individual species diffuse preferentially according to their molecular mass, with low-mass species generally moving toward the warm end [*Grew and Ibbs*, 1953]. This effect, called thermal diffusion fractionation, has been observed in firn [*Severinghaus et al*., 2001] and sand dunes [*Severinghaus et al*., 1996] as well as measured extensively in laboratory experiments [*Grachev and Severinghaus*, 2003; *Kawamura et al*., 2013]. At UZ depths below the influence of the seasonal cycle, the vertical temperature difference between the surface and a depth *z*, is given by the geothermal gradient, Γ, multiplied by z. This temperature difference leads to thermal diffusion fractionation of a magnitude (in ‰) given by

$$\delta_{\mathrm{therm}}(i,z) = -\Omega_i \Gamma z \tag{5}$$

where Ω_i is the thermal diffusion sensitivity of ratio *i* in ‰ K^{-1}, Γ is the geothermal gradient in K m^{-1}, and *z* is depth in m.

1.1.3. Diffusion Against Vertical Fluxes

The deep UZ (relative humidity → 100%) diffusively transports water vapor upward to the drier lower atmosphere at steady state. From observations of O_2 and N_2 isotope ratios in a sand dune, *Severinghaus et al*. [1996] first discovered that this upward flux of water vapor induces kinetic fractionation of "stagnant" UZ gases, leading to a depletion of heavy relative to light isotopes within the moist UZ. This phenomenon, known as the "water vapor flux fractionation effect," results because of the lower binary diffusivities of heavy isotopologues relative to light isotopologues diffusing against water vapor [*Fuller et al*., 1966]. In other words, the upward flux of water vapor advects stagnant UZ gases (e.g., noble gases) upward, and at

steady state this advective transport is balanced by downward diffusive transport, as required by mass conservation. This diffusive transport is faster for light isotopologues, leading to their steady state enrichment vs. heavy isotopologues, relative to the free atmosphere. As derived in *Severinghaus et al*. [1996], the magnitude of this effect on a gas ratio, *i*, is approximated (in ‰) by

$$\delta_{\mathrm{diff}}(\mathrm{i},\mathrm{z}) \approx \left[\left(\frac{1-\chi_{\mathrm{k}}(\mathrm{z})}{1-\chi_{\mathrm{k}}(0)}\right)^{\frac{D_{b-k}}{D_{a-k}}-1}-1\right]\times 10^{3}‰ \quad (6)$$

where *a* and *b* are the heavy and light species, respectively, of ratio *i*, *k* is the steady state diffusing gas (e.g., water vapor), $\chi_k(z)$ is the mole fraction of gas *k* at depth *z* in the UZ (in m), and D_{a-k} and D_{b-k} are the binary diffusivities [*Fuller et al*., 1966] of gas species *a* and *b* against gas *k*, respectively, in $m^2\ s^{-1}$. This approximation is valid to within ~0.001‰ [*Severinghaus et al*., 1996]. At ADRS, a substantial deep source of CO_2 similarly leads to steady state upward diffusion of CO_2 [*Walvoord et al*., 2005]. In our steady state fractionation model at ADRS, δ_{diff} is composed of fractionation due to upward diffusion of both H_2O and CO_2. In Figure 1, the resulting two components of δ_{diff} are shown independently as δ_{H2O} and δ_{CO2}.

Because the UZ depth range considered this study (below 20 m) is saturated with respect to water vapor, changes in χ_{H2O} with depth are slight and purely a function of temperature. Because temperature increases with depth along the geothermal gradient, χ_{H2O} also increases because warmer UZ air has a higher saturation vapor pressure via the Clausius-Clapeyron relation. Water vapor flux fractionation, therefore, is relatively insensitive to depth (Figure 1).

1.2. Study Area: ADRS

The ADRS is located adjacent to a closed, state-managed, LLRW disposal site in the Amargosa Desert in Nye County, Nevada (Figure 2). The UZ at ADRS, composed mostly of sand and gravel, is about 110 m thick at the locations of the two bores sampled in this study: UZB-2 and UZB-3. Sedimentary layering at ADRS leads to higher lateral than vertical diffusivity, as inferred from a gas tracer study carried out from 2005 to 2006 [*Green et al*., 2015]. Mean annual surface temperature, relative humidity, and ambient air pressure at the site are 21.4°C, 29.2%, and 91.8 kPa, respectively, according to hourly measurements made over an 8 year span [*Johnson et al*., 2002, 2007]. The geothermal gradient at bores UZB-2 and UZB-3 is 0.046 K m^{-1} [*Walvoord et al*., 2004]. Bores UZB-2 and UZB-3 contain ports spaced irregularly between the surface and depths of

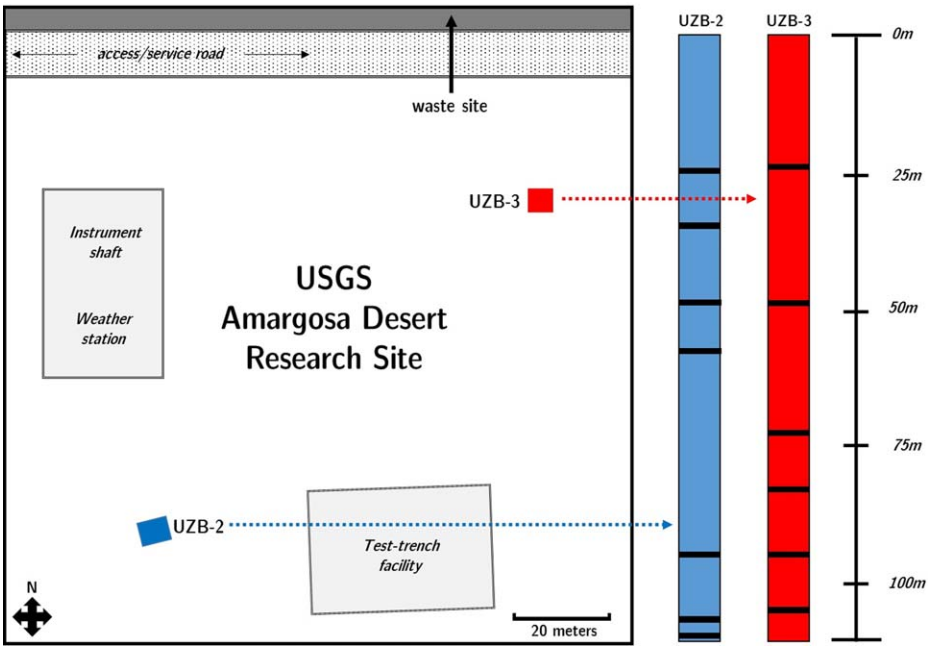

Figure 2. Amargosa Desert Research Site (ADRS) map showing locations of unsaturated zone sampling bores UZB-2 and UZB-3, weather station, edge of the closed, low-level waste site, and sampling depths.

108.8 and 103.9 m, respectively. These ports consist of nylon tubing connected to 30 cm vertical screens in gravel sealed at the top and bottom by bentonite. The nylon tubing at each sampling port extends up to stations at the surface of each bore where each gas line is kept closed to the atmosphere while not in use. CO_2 concentration profiles at UZB-2 and UZB-3 below ~50 m similarly increase monotonically to ~1% by volume above the water table [*Walvoord et al*., 2005]. Because a middepth CO_2 peak at UZB-3 is likely due to waste-induced microbial activity [*Stonestrom et al*., 2004], we take the UZB-2 CO_2 profile as indicative of steady state in both bores (Appendix B).

UZB-3 is located nearer than UZB-2 to the waste site and as a result, any thermal or chemical anomalies in the UZ below the waste affect UZB-3 samples more than UZB-2. Although persistent horizontal temperature differences are unlikely in most UZs, heat production within the buried waste next to ADRS is possible due to high microbial activity [*Mayers et al*., 2005]. The effect of this potential lateral temperature structure on measured isotope ratios is discussed in section 4.1. Unlike UZB-2, in addition to the nylon sampling tubes, UZB-3 contains a ~5 cm diameter PVC pipe extending to a 1.5 m tall screened interval straddling the water table. Prior to the April 2015 sampling, this pipe was fitted with a PVC cap (supporting information Figure S1a). Extensive UZ gas sampling to characterize contaminants was done prior to noble gas sampling in April 2015, potentially inducing a downward pressure gradient and drawing atmospheric air to the water table through this unsealed cap. In January 2016, an adjustable rubber-sealed cap (supporting information Figure S1b) was installed to prevent the UZB-3 pipe from being a potential conduit to the atmosphere.

2. Methods

2.1. Steady State Fractionation Model

Expected values of δ_{NET} in the ADRS UZ are time invariant. We model the individual components δ_{NET} (Figure 1) using equation (2), evaluated via equations (4)–(6). The model is constructed using mean site parameters at ADRS (pressure, temperature, geothermal gradient, surface humidity, and CO_2) and their estimated uncertainties. The 2σ uncertainty of the model is estimated by 1000 Monte Carlo simulations with assumed Gaussian variance of site parameters.

In this steady state model, $T(z)$ (equation (4)) is given by $T_{surf} + \Gamma z$, where T_{surf} is mean annual surface temperature. In the model, T_{surf} is 21.4 ± 0.4°C [*Johnson et al*., 2002, 2007], Γ is 0.046 ± 0.005 K m^{-1} [*Walvoord et al*., 2004], and z ranges from 20 to 110 m below the surface with uncertainty assumed to be ±93 cm (1σ). The uncertainty in sample depth results from the vertical extent of the UZ pore space from which samples were drawn. We estimated this value to be the radius of a sphere with volume equal to the ~2 L min^{-1} pumping rate (section 2.2) multiplied by the average pumping time elapsed after flushing and sample collection (~40 min) divided by the mean ADRS porosity of 0.24 [*Andraski*, 1996]. Thermal diffusion sensitivities (equation (5)) are based on published values for isotopes of Ar [*Grachev and Severinghaus*, 2003], Kr [*Kawamura et al*., 2013], and Xe [*Kawamura et al*., 2013]. Binary diffusivities (equation (6)) are calculated according to the method of *Fuller et al*. [1966] as described in *Reid et al*. [1977].

At ADRS, we assume water vapor saturated air throughout the entire modeled UZ (20–110 m) and 0.005 ± 0.001 mole fraction of water vapor at the surface [*Johnson et al*., 2002, 2007]. ADRS also has a constant upward flux of CO_2 driven by a mole fraction of ~0.01 at the water table. We parameterize the CO_2 profile at ADRS based on past UZB-2 measurements and their uncertainties (Appendix B) [*Walvoord et al*., 2005].

2.2. Unsaturated Zone Gas Sampling

Gas samples were collected from seven depths at UZB-2 and six depths at UZB-3 in April 2015 (Figure 2). Because the focus of this study is steady state fractionation, we limited the influence of the seasonal temperature and moisture changes, which affect only the top few meters of the unsaturated zone, by exclusively sampling below 20 m. Two replicate 2 L glass flasks were filled from each depth. Each flask was filled by purging the 4 mm (internal diameter) tubing 20 times before pumping UZ gas through thermally insulated fluorocarbon tubing (Dekoron®) at ~2 L min^{-1} for 10 min. A magnesium perchlorate trap was used to remove moisture upstream of the tubing. The tubing included ~1 m long coils both upstream and downstream of the flask to prevent ambient air from entering the flask during the 10 s between turning off the pump and closing the valves. Supporting information Figure S5 contains a diagram of the sample collection

setup. At UZB-2, samples were collected at depths of 24.1, 34.1, 47.9, 57.6, 94.2, 106.4, and 108.8 m. At UZB-3, samples were collected at depths of 23.8, 48.6, 72.1, 82.4, 94.1, and 103.9 m.

In May 2016, four deep ports were resampled to test the hypothesis of atmospheric contamination during the 2015 sampling. Samples were collected from 106.4 and 108.8 m at UZB-2 and 82.4 and 103.9 m at UZB-3. One 2 L glass flask was filled from each of these four depths following the same procedure used in the prior year.

2.3. Sample Preparation and Analysis

Stable isotope ratios of argon ($\delta^{40}/_{36}$Ar, $\delta^{40}/_{38}$Ar), krypton ($\delta^{86}/_{82}$Kr, $\delta^{86}/_{83}$Kr, and $\delta^{86}/_{84}$Kr), and xenon ($\delta^{136}/_{129}$Xe, $\delta^{134}/_{129}$Xe, and $\delta^{132}/_{129}$Xe) were measured in the Noble Gas Isotope Laboratory at Scripps Institution of Oceanography, broadly following techniques of *Kawamura et al.* [2013]. Each measured aliquot was extracted from the sampling flask into a $\sim$100 cm^3 evacuated volume before being transferred through a water trap (–80 to $-$100°C) into a dip tube immersed in liquid helium.

The dip tube was then connected to a secondary vacuum line and gettered at 900°C with SAES Zr/Al getter sheets before being transferred to a secondary dip tube immersed in liquid helium. This dip tube was then analyzed on a Thermo-Finnigan MAT 253 dual inlet mass spectrometer after allowing a minimum of 3 h of equilibration.

Sample analysis was completed in two phases: one main campaign from September 2015 to January 2016 (campaign A) and a subsequent minor campaign from May to June 2016 (campaign B). Campaign A included measurement of six to seven replicate aliquots from each depth sampled in April 2015. Campaign B included three replicate aliquot measurements from each of the four depths sampled in May 2016 as well as reanalysis of two replicate aliquots (collected in April 2015) from the deepest ports of both UZB-2 and UZB-3 (see Appendix A). The run sequence on the mass spectrometer was modified for campaign B in order to avoid an artifact in Ar isotopic measurements caused by low measurement pressures and validate an apparent pressure sensitivity correction to previous Ar isotopic measurements (see Appendix A).

Measured isotope ratios were normalized to the mean of dry atmospheric air replicates collected off the Scripps pier in La Jolla, CA. These replicate aliquots were collected, prepared, and analyzed throughout each measurement campaign in the same manner as other sample aliquots (11 replicates during campaign A and 6 during campaign B). During campaign A, three aliquots from a flask of air collected from the surface at ADRS were measured, using the same equipment used for UZ sampling. All mean isotope ratios measured in ADRS surface samples agreed (within $2\sigma_{pooled}$) with the mean pier air values, confirming that our sampling technique does not fractionate noble gas isotopes.

During campaign A, five blocks (25 integration cycles per block, 26 s integration time) of xenon and krypton isotopes each were measured at 350 mV (mass 132) and 800 mV (mass 82), respectively. Four blocks of argon isotopes (16 integration cycles per block, 16 s integration time) were measured at 5500 mV for mass 36 (actual intensities dropped to 3000 mV, see Appendix A). Inlet gas pressures were $>$40 mbar during Kr and Xe analysis, but as low as 20 mbar during Ar measurements due to consumption of the aliquot during the $\sim$10 h run. During campaign B, xenon and krypton isotopes were measured in the same manner, except two 25 cycle Kr isotope blocks were removed to accommodate higher pressure (11,000 mV, $\sim$45 mbar inlet pressure) argon measurements. Incomplete gettering of several campaign B aliquots resulted in isobaric interference with Xe isotopes. Mass spectrum comparisons between ungettered UZ and standard gases revealed a non-Xe peak in UZ gas centered near mass 134. We surmise that this contaminant was from known abundant chlorofluorocarbon species in the Xe mass range in ADRS UZ air [*Baker et al.*, 2012]. In campaign B, we observed large disagreement among replicate aliquots (e.g., $\sim$1‰ for $\delta^{136}/_{129}$Xe) which also showed characteristically high $\delta^{134}/_{129}$Xe, implying isobaric interference in these measurements. We concluded that getter sheet manufacturing inconsistencies led to incomplete gettering. In response, we increased the number of getter sheets used in campaign B to 56 (from 36 in campaign A) to ensure complete gettering. Measurements of aliquots affected by isobaric interference have been excluded and aliquots gettered with additional sheets showed improved Xe isotope agreement, with pooled standard deviations (σ_{pooled}) comparable to those of campaign A (Table 1). Measured isotope ratios were corrected for pressure imbalances between the pressure-adjusting bellows containing sample and standard gases via

Table 1. Isotope Ratio Weights in Inverse Model, Mass Differences, Thermal Diffusion Sensitivities, and Measurement Uncertainties (σ_{pooled}) for Measurement Campaigns A and B

Isotope Ratio, i	$\delta^{40}/_{36}$	$\delta^{40}/_{38}$	$\delta^{86}/_{82}$	$\delta^{86}/_{83}$	$\delta^{86}/_{84}$	$\delta^{136}/_{129}$	$\delta^{134}/_{129}$	$\delta^{132}/_{129}$
Gas	Ar	Ar	Kr	Kr	Kr	Xe	Xe	Xe
W_i	1	1.03	4.10	4.13	4.15	5.19	5.15	5.11
Δm_i (g mol^{-1})	4	2	4	3	2	7	5	3
Ωi (‰ K^{-1})[a]	0.043	0.021	0.010	0.008	0.005	0.014	0.010	0.006
σ_{pooled} A (‰)	0.017	0.009	0.021	0.027	0.017	0.067	0.065	0.042
σ_{pooled} B (‰)	0.004	0.006	0.028	0.022	0.021	0.069	0.047	0.035

[a]Thermal diffusion sensitivities for argon [*Grachev and Severinghaus*, 2003], krypton [*Kawamura et al.*, 2013], and xenon [*Kawamura et al.*, 2013] isotopes.

pressure imbalance sensitivity tests run every 1–2 weeks throughout each campaign. The pooled standard deviations of isotope ratios measured in each campaign are given in Table 1.

2.4. Inverse Model Applications

At ADRS, known UZ parameters such as vertical gradients of temperature, water vapor, and CO_2 were used to directly estimate the magnitude of steady state noble gas isotope fractionation using a forward model (section 1.1). In principle, however, measured noble gas isotope ratios could be used to solve an inverse problem in order to estimate one or more UZ parameters. Here we introduce an inverse approach for two applications: (1) to resolve the extent of mixing with atmospheric air introduced at depth (specific to ADRS, section 3.2) and (2) to estimate the past depth of a gas parcel within a UZ from reconstructed steady state UZ noble gas isotope ratios (e.g., from paleorecharge sequestered as deep groundwater, a potential future application discussed in section 4.2).

For the first application, determining atmospheric admixture extent of each sample, $f_{atm}(z,b)$, a cost function, $C(z,b)$ is defined as follows:

$$C(z,b)=\sum_{i=1}^{N}\left(\frac{\delta(i,z,b)_{meas}-\ (1-f_{atm}(z,b))\delta(i,z,b)_{model}}{\sigma(i,z,b)}\right)^2 \tag{7}$$

for a sample collected at depth, z, in bore, b, where i is one of $N=8$ independent isotope ratios measured in this study, $\delta_{meas}(i,z,b)$ and $\delta_{model}(i,z,b)$ are replicate-mean measured and steady state modeled (equation (2)) isotope ratios (in ‰), respectively, and $\sigma(i,z,b)$ is the quadrature sum of measurement and model standard deviations of isotope ratio i (in ‰). Because $\delta_{model}(i,z,b)$ is fully determined based on known ADRS UZ parameters, the eight $\delta_{meas}(i,z,b)$ values at each bore-depth pair comprise an overdetermined system of equations with one unknown: $f_{atm}(i,z,b)$. For 1000 Monte Carlo simulations, in which each $\delta_{meas}(i,z,b)$ is perturbed with Gaussian random noise with zero mean and standard deviation equal to $\sigma(i,z,b)$, $f_{atm}(i,z,b)$ is solved for by minimizing equation (7), which amounts to a linear least squares approach.

For the second application, estimating depth from a suite of measured or inferred UZ noble gas isotope ratios, we define an alternate cost function that weights individual isotope ratios based on their relative sensitivity to gravitational settling. In this case, depth is treated an unknown variable and is estimated through cost-function minimization (nonlinear least squares). For each sample, $C(z,b)$ is defined similarly to equation (7):

$$C(z,b)=\ \sum_{i=1}^{N} W_i\left(\frac{\delta(i,z,b)_{meas}-\ \delta(i,z,b)_{model}}{\sigma(i,z,b)}\right)^2 \tag{8}$$

where W_i is the weighting factor (defined below), $\sigma(i,z,b)$ is the measurement standard deviation, and $\delta(i,z,b)_{model}$ is calculated (equations (2) and (4)–(6)) using a modern value for Γ, prescribing or neglecting a vertical CO_2 gradient (as described in section 4.2), and leaving the other two variables in the model (depth and water vapor gradient) as free parameters. Equation (8), therefore, comprises a system of eight equations and two unknowns. While the steady state vertical CO_2 gradient at ADRS is substantial, we note that UZ depth estimation would be most applicable in settings without high deep CO_2 concentrations (and without correspondingly strong CO_2-flux fractionation). In section 4.2, we examine the sensitivity of UZ depth estimates (via equation (8)) to prescription of a steady state UZ CO_2 profile or omission of CO_2-induced fractionation altogether.

Because the relative contribution of water vapor flux fractionation is small for each measured isotope ratio, we do not expect to accurately resolve past UZ water vapor mole fraction differences between the water table and surface using heavy noble gas isotopes. Instead, this inverse model only roughly estimates the small magnitude of water vapor flux fractionation in order to isolate the contribution of gravitational settling fractionation and therefore resolve depth. Indeed, our decision to measure Ar, Kr, and Xe isotopes was motivated by the expected high sensitivity of these isotope ratios to gravitational settling fractionation. To further increase the composite sensitivity of a suite of Ar, Kr, and Xe isotopes to depth within the UZ, we define a weighting W_i in the following manner:

$$W_i = \frac{Q_i}{Q_{40/36}} \tag{9}$$

where Q_i represents the ratio of gravitational settling fractionation per meter to thermal diffusion fraction per Kelvin for isotope ratio i, such that weights are calculated relative to this ratio for $\delta^{40}/_{36}$Ar. Formally, Q_i is defined:

$$Q_i = \frac{\partial \delta_{grav,i}/\partial z}{\Omega_i} \tag{10}$$

where $\delta_{grav,i}$ and Ω_i are calculated at 293 K. $\partial\delta_{grav,i}/\partial z$ is given by its first Taylor approximation:

$$\partial \delta_{grav,i}/\partial z = \frac{\Delta m_i g}{RT} \tag{11}$$

where Δm_i is the mass difference between heavy and light isotopes for isotope ratio, i, in amu, R is the ideal gas constant in J K^{-1} mol^{-1}, and T is temperature in K.

Table 1 contains the weights, mass differences, and measurement precision of isotope ratios measured in this study. Because δ_{grav} is independent of atomic mass (equation (4)) and $|\delta_{diff}|/|\delta_{NET}|$ decreases with atomic mass, $|\delta_{grav}|/|\delta_{NET}|$ increases with atomic mass. Therefore, isotope ratios of heavy gases are weighted more than those of light gases. Specifically, Xe and Kr isotope ratios are respectively weighted roughly 5 and 4 times more than Ar isotope ratios. $|\delta_{diff}|/|\delta_{NET}|$ decreases with atomic mass because D_{a-k}/D_{b-k} approaches unity. In other words, the depth signal of interest is strongest in the xenon isotopes.

3. Results

3.1. Measured Isotope Ratios in April 2015 Samples

Replicate-mean δ values of all eight isotope ratios measured at all depths below 60 m fell below modeled values (i.e., ratios were depleted in the heavier isotope, Figure 3). Additionally, replicate-mean δ measurements across all depths and both bores were always greater than or equal to atmospheric air ($\delta = 0$), within 1σ. The degree to which measured values deviated from the model below 60 m was substantially higher at UZB-3 than UZB-2. Figure 3 shows replicate-mean measured δ values (open markers) at each of the 13 sampled depths alongside the modeled steady state isotopic profiles (δ_{NET}) described in section 1.1.

The UZB-3 sample nearest to the water table (103.9 m depth) was effectively atmospheric with respect to the eight measured isotope ratios. Normalizing each ratio by its isotopic mass difference (e.g., 4 for $\delta^{40}/_{36}$Ar), the replicate-mean, ratio-mean, per-mass-unit δ value was $0.004 \pm 0.009‰$ amu^{-1} at this depth. Above this depth, the next three sampled UZB-3 depths (94.1, 82.4, and 72.1 m) monotonically decreased in deviation from the model (increased in δ value) in all eight measured isotope ratios. Though less extreme, a similar decrease in deviation from the model with height above the water table was apparent in UZB-2.

We hypothesize that extensive sampling from the UZ in the week before our April 2015 field study induced bulk flow of atmospheric air through an unsealed PVC pipe (supporting information Figure S1) directly into the deep UZ above the water table at UZB-3. Pumping at shallower UZB-3 depths prior to our sampling would have spread this unfractionated atmospheric air upward from ~110 m depth, where it would have diluted the preexisting UZ air, until ~50 m depth, where contamination was effectively undetectable (section 3.2). This volume of atmospheric air between 50 and 110 m would also have spread laterally outward and affected the deeper portion of UZB-2. We tested this hypothesis in two ways. First, we ran the inverse model (section 2.4) with measured δ values and prescribed ADRS conditions (surface pressure, temperature,

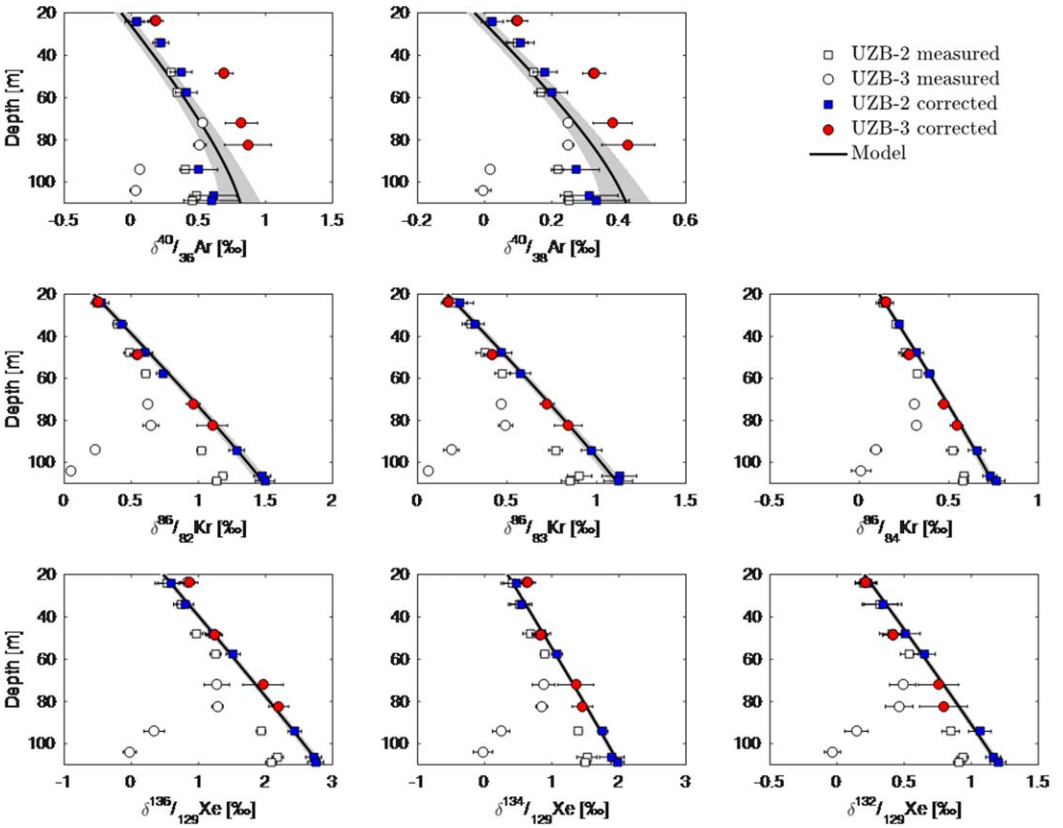

Figure 3. Measured and atmospheric contamination-corrected Ar, Kr, and Xe isotope ratios in April 2015 ADRS unsaturated zone samples. Corrected values are plotted for all depths except for the two deepest ports at UZB-3, at which the atmospheric contamination fraction is too large (>80%) to meaningfully remove it and estimate uncontaminated values. Error bars on corrected values indicate 2σ uncertainty based on atmospheric contamination percentage estimated by 1000 Monte Carlo simulations. Error bars on uncorrected measurements indicate 2σ uncertainty based on six to seven replicate aliquot measurements at each depth. Shaded gray region around mean modeled profiles indicates 2σ model uncertainty from 1000 Monte Carlo simulations.

absolute humidity, geothermal gradient, and CO_2 profiles) to solve for the fraction of atmospheric contamination at each depth. We tested for model convergence around a narrow range of likely atmospheric contamination percentages at each depth (section 3.2, Appendix C). Second, we returned to ADRS in May 2016 after installation of a gas-tight seal in the UZB-3 PVC pipe and collected samples from two deep ports in UZB-2 (106.4 and 108.8 m) and UZB-3 (82.4 and 103.9 m) to determine if isotope ratios had progressed toward the steady state modeled δ values.

3.2. Atmospheric Contaminant Determination and Correction

The percentage of atmospheric contamination was estimated at each depth using 1000 Monte Carlo simulations of the inverse model described by equation (7). Replicate-mean δ values were perturbed with normally distributed measurement uncertainties as described in section 2.4 in order to estimate the mean and uncertainty of atmospheric contaminant fractions in each sample, $f_{atm}(z,b)$. Figure 4 shows the results of atmospheric contamination estimation in April 2015 samples. The atmospheric contaminant percentage in each bore decreased between the water table and ~50 m depth. At UZB-3, the deepest sample (103.9 m) was estimated to be 98 $\pm$ 1% pure atmospheric air.

To qualitatively evaluate the goodness of fit among the eight measured isotope ratios, we corrected the replicate-mean δ values at each depth for mixing with the estimated concentration of atmospheric air. Figure 3 (filled markers) shows these air contamination-corrected profiles and their good general agreement with the steady state model. Due to large atmospheric contamination in the two deepest UZB-3 samples, the remaining nonatmospheric signal is too small to meaningfully estimate and these samples are therefore excluded from Figure 3.

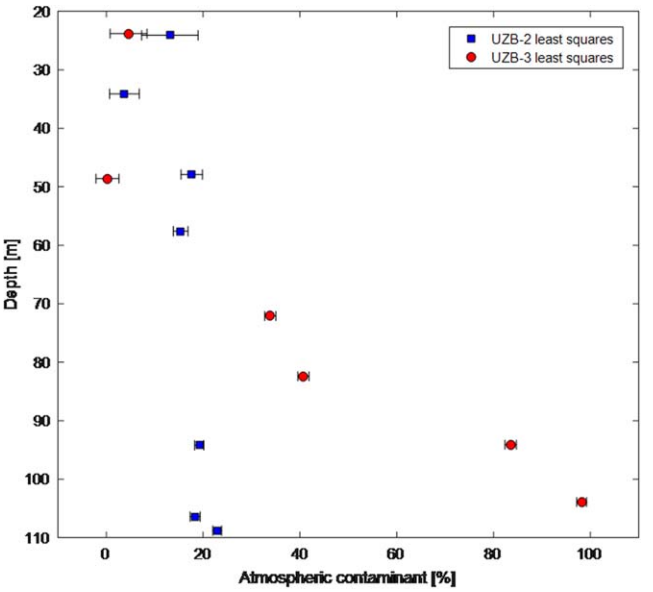

Figure 4. Inferred atmospheric contamination percentage at measured sample depths. Atmospheric contamination is determined by weighted least squares based on the deviations between the eight measured and modeled noble gas isotope ratios at each depth. Error bars indicate 1σ uncertainty based on 1000 Monte Carlo simulations with variance prescribed by measurement and model uncertainties.

We more quantitatively assessed the least squares estimation of atmospheric contamination by independently calculating alternate contamination estimates based on individual isotope ratios measured in each sample. The details of the analysis are presented in Appendix C. The 95% confidence intervals of individual atmospheric contaminant fraction estimates overlap for the six Xe and Kr isotope ratio-based estimates for all samples collected at ADRS (supporting information Figure S6). In 6 of 13 total samples, atmospheric contaminant fractions estimated independently by Ar isotope ratios diverge slightly from estimates derived independently from Kr and Xe isotope ratios. Given that Ar is substantially more sensitive to thermal diffusion and CO_2-flux fractionation, uncertain and potentially large horizontal thermal gradients as well as uncertainty concerning the steady state CO_2 profile may explain why Ar isotopes sometimes yield differing atmospheric contaminant estimates. We further discuss these complications for modeling Ar isotope fractionation at ADRS in section 4.1.

3.3. Measured Isotope Ratios in May 2016 Samples

The mean δ values measured in three replicate aliquots from four deep samples collected in May 2016 (UZB-2: 106.4 and 108.8 m; UZB-3: 82.4 and 103.9 m) are shown in Figure 5. Whereas isotope ratios were relatively unchanged from April 2015 in three of these four samples, all eight replicate-mean δ values at 103.9 m in UZB-3 increased substantially toward the steady state model. We interpret these results as evidence of partial diffusive resettling after the atmospheric contamination event in April 2015 and suggest that the sealed cap on the UZB-3 PVC pipe (supporting information Figure S1) had prevented further atmospheric contamination.

We note that relative to their April 2015 deviation from the steady state model, δ values of Ar isotopes (faster diffusivity) increased more than those of Kr and Xe isotopes (slower diffusivity) in the UZB-3 103.9 m sample. With incomplete knowledge of the three-dimensional structure of effective diffusivity at ADRS and the initial amount and location of atmospheric air contamination, we cannot quantify the degree of diffusive resettling. Nonetheless, we note generally that the pattern of isotopic changes from April 2015 to May 2016 is consistent with our hypothesized contamination event and steady state model.

The smaller April 2015 to May 2016 changes in UZB-2 and at 82.4 m in UZB-3 may be explained by less initial atmospheric contamination (below 50% at each of these depths, Figure 4). The driver of isotopic rebound after the contamination, as hypothesized, is equivalent to the model-measurement discrepancy, $\Delta\delta(i,z,b) = \delta(i,z,b)_{2015} - \delta(i,z,b)_{model}$. Because $\Delta\delta(i,z,b)$ decreases in magnitude above and laterally away from the bottom of UZB-3, the steeper spatial gradient, $\nabla\cdot(\Delta\delta(i,z,b))$ in the deepest portion of UZB-3 versus the overlying depths would lead to higher diffusive transport according to Fick's law. As a result, there is less isotopic change from April 2015 to May 2016 at the considered.

4. Discussion

4.1. Noble Gas Isotopes as Tracers at ADRS

Measured isotope ratios of Ar, Kr, and Xe in UZ samples collected at the ADRS deviated from expected steady state values in a systematic way. All April 2015 measured isotope ratios (δ values) at all depths below

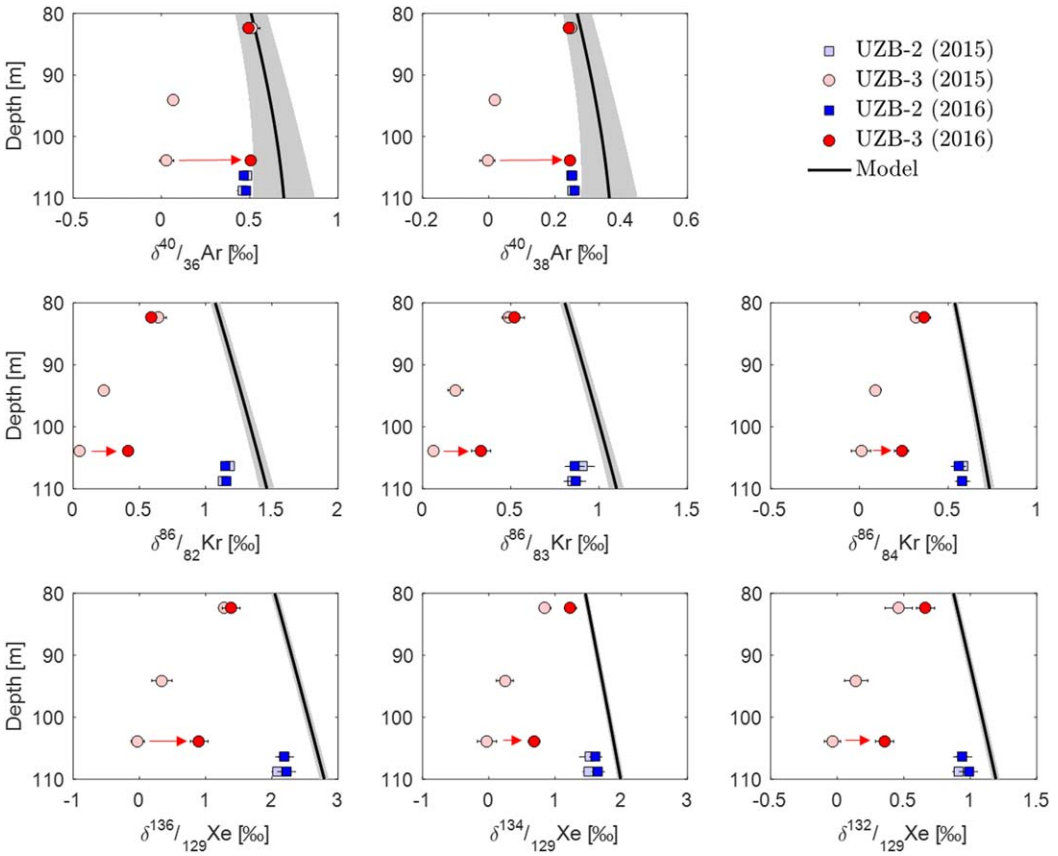

Figure 5. Measured Ar, Kr, and Xe isotope ratios in April 2015 (light colors) and May 2016 (dark colors) ADRS unsaturated zone samples. May 2016 measurements were made on samples collected at 106.4 and 108.8 m in UZB-2 and 82.4 and 103.9 m in UZB-3. Red arrows highlight the development of the deepest UZB-3 sample toward the expected modeled values between the 2015 and 2016 measurements. Error bars on April 2015 samples indicate 2σ uncertainty based on six to seven replicate aliquot measurements at each depth. Error bars on May 2016 samples indicate 2σ uncertainty from pooled variance of measurement campaign B (N = 22). Shaded gray region around mean modeled profiles indicate 2σ model uncertainty from 1000 Monte Carlo simulations.

60 m were lower than expected, especially at UZB-3 where the deepest sample (103.9 m) closely approximated atmospheric noble gas isotopic composition (Figure 3). We applied a weighted inverse model (section 2.4) to estimate the fraction of atmospheric contaminant at each depth, which showed a monotonic decrease in contaminant fraction with height above the water table until ~50 m (Figure 4). Subsequent analysis on a subset of deep ports resampled in May 2016 showed substantial development of isotope ratios in the deepest UZB-3 sample toward the expected steady state concentration (Figure 5). We interpret deviations of deep UZ samples from the expected steady state profile as evidence of an atmospheric contamination event at the UZB-3 water table prior to sampling in April 2015.

Above 60 m, measured δ values were much nearer to the steady state model, except for Ar isotopes at both UZB-2 and UZB-3. Ar isotope δ values in UZB-3 especially were higher than expected, consistent with unexpected thermal diffusion fractionation, possibly associated with heat produced by microbial activity within the buried waste at the neighboring waste disposal facility [*Stonestrom et al.*, 2004]. A waste-generated heat source could lead to a horizontal temperature gradient, driving thermal diffusion fractionation. Because lighter isotopes diffuse preferentially toward warmer temperatures [*Grew and Ibbs*, 1953], δ values would increase at UZB-3 and, to a lesser extent, at UZB-2, which is farther from the waste. Because the thermal diffusion sensitivities (per mass unit) are more than 4 times greater for isotopes of Ar [*Grachev and Severinghaus*, 2003] than Kr and Xe [*Kawamura et al.*, 2013], we suggest that the poorer fit of corrected Ar δ values to the model is a consequence of a two-dimensional horizontal thermal structure, plausibly due to the heat generated by decomposition in the horizontally adjacent waste dump. Uncertainty in the steady state upward CO_2 flux may also explain why independent Ar isotope-derived estimates of atmospheric contamination in some cases diverge from those of Kr and Xe isotopes (Appendix C), since Ar isotopes are more

sensitive to CO_2-flux fractionation (high $|\delta_{CO2}|/|\delta_{NET}|$). A more complete correction would estimate and remove the influence of horizontal temperature gradients as well as atmospheric contamination. However, due to the low sensitivity to thermal diffusion fractionation (small $|\delta_{therm}|/|\delta_{NET}|$) among the isotope ratios measured in this study, the inverse model (described in section 2.4) could not reasonably resolve horizontal temperature gradients. The sensitivity of Ar isotopes to processes other than gravitational fractionation justifies its relative downweighting in the inverse model we propose for depth estimation.

4.2. Potential Applications of Noble Gas Isotopes in Paleogroundwater

Preferential-flow features that provide direct conduits between the water table and atmosphere will limit the proposed application to unfissured unsaturated zones, like that present at the ADRS [*Green et al*., 2015; cf. *Weisbrod et al*., 2009; *Mourzenko et al*., 2014]. In the absence of these uncommon disruptions, we expect noble gas isotopes to follow the steady state model outlined in section 1.1. The good agreement of atmospheric contaminant-corrected ADRS measurements with the steady state model adds confidence to this expectation.

One potential application of this suite of eight noble gas isotope ratios, measured in paleogroundwater, is its capacity to estimate past water table depth. Over long time scales, groundwater with dissolved UZ gases is sequestered from the atmosphere in confined aquifers. Because the heavy noble gas isotopes in these paleogroundwaters were inherited from a past UZ, they contain information about gravitational settling fractionation and therefore past UZ thickness (i.e., water table depth).

The reconstruction of steady state UZ Ar, Kr, and Xe isotope ratios from measurement of dissolved gases in groundwater would be complicated by fractionation during dissolution [*Tempest and Emerson*, 2013]. This additional fractionation influences measured isotope ratios in two ways: (1) the slightly different isotopic solubilities induces "solubility fractionation" at equilibrium and (2) the partial dissolution and potential reequilibration of so-called "excess air" may induce further fractionation. At present, solubility fractionation factors for isotopes of Xe and Kr are unknown and would need to be empirically determined prior to the application of this proposed paleo water table depth estimation tool. The solubility fractionation factor for $\delta^{40}/_{36}$Ar is $\sim$1.07‰ [*Tempest and Emerson*, 2013]. To constrain the fractionation due to excess air, a noble gas groundwater excess air model would need to be extended to Ar, Kr, and Xe isotopes. The closed-system equilibration (CE) model [*Aeschbach-Hertig et al*., 2000], which has been widely used for paleotemperature reconstruction, assumes partial dissolution of persistent entrapped air in solubility equilibrium with groundwater. This model would be applicable to isotopes and only requires knowledge of solubility fractionation factors for all measured isotope ratios. Another common excess air model, the partial reequilibration (PR) model [*Stute et al*., 1995], assumes diffusive reequilibration after complete dissolution of entrapped air. The extension of this model to isotopic measurements would require empirical determination of kinetic fractionation factors for each isotope ratio across the air-groundwater interface. This kinetic fractionation factor has been measured for $\delta^{40}/_{36}$Ar, but with wide disagreement between two independent studies [*Tyroller et al*., 2014; *Tempest and Emerson*, 2013]. We suggest that future attempts to quantify past water table depths from measurement of dissolved noble gas isotopes in paleogroundwater begin with samples of known low excess air concentrations and good fit of bulk noble gas concentrations using the CE model, to reduce potential sources of uncertainty.

By accounting for fractionation due to dissolution, measured dissolved noble gas isotope ratios could be converted to paleo-UZ noble gas ratios. Paleo water table depth could then be estimated by using the weighted inverse model described in section 2.4 (equation (8)). Ar isotope measurements at ADRS displayed poorer agreement with the model than did Kr and Xe isotopes, likely due in part to uncertainty about the magnitude of the steady state CO_2 flux. Because the proposed water table depth estimation method would be most successful at sites with known weak UZ CO_2 fluxes, we investigated the sensitivity of the inverse model to the inclusion/exclusion of Ar isotopes and CO_2-flux fractionation.

This sensitivity test was carried out using synthetic data produced by the forward UZ fractionation model (section 1) run at ADRS environmental conditions (geothermal gradient, temperature, pressure, humidity, and CO_2). As outlined in the method section, we ran 1000 Monte Carlo simulations at each depth from 20 to 110 m perturbing the modeled isotopic values with normally distributed random values of zero mean and standard deviation equal to pooled measurement standard deviations (campaign A). For each simulation, we estimated depth under four configurations of the inverse model: (1) using all eight isotope ratios

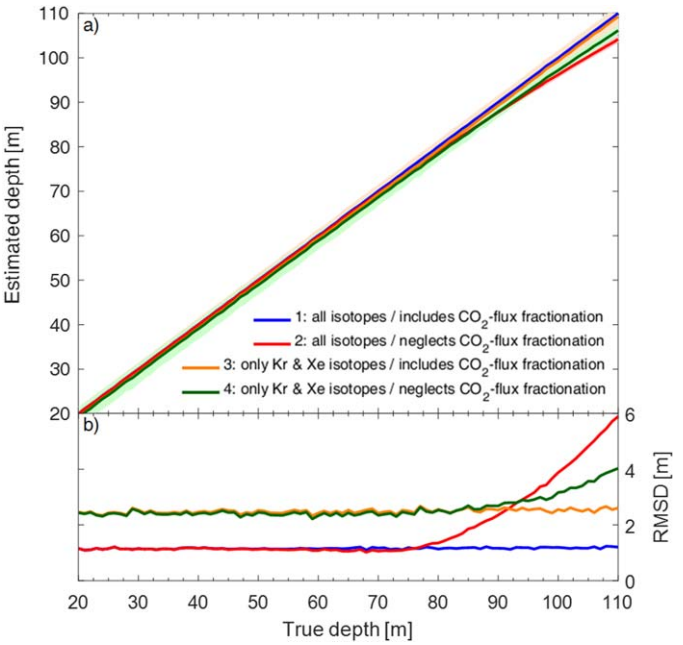

Figure 6. Comparison of actual to estimated sample depths in sensitivity test of inverse model run under four scenarios at ADRS environmental conditions (temperature, pressure, humidity, CO_2, and geothermal gradient). Scenarios 1 and 2 utilize all eight noble gas isotope ratios considered in this study as constraints for the inverse model. Scenarios 3 and 4 exclude argon isotope ratios. Scenarios 2 and 4 exclude CO_2-flux fractionation to assess the potential bias for neglecting CO_2 fractionation in a paleo UZ for which CO_2 profiles would not be known a priori.

and accounting for CO_2-flux fractionation, (2) using all eight isotope ratios but neglecting CO_2-flux fractionation, (3) using only Kr and Xe isotopes and accounting for CO_2-flux fractionation, and (4) using only Kr and Xe isotopes and neglecting CO_2-flux fractionation. Figure 6 shows the ability of the inverse model to estimate true depths under each scenario.

Under all scenarios, root-mean-squared deviations (RMSD) between synthetic measurements and the steady state model are less than 6 m. Scenario 2, which includes Ar isotopes and neglects CO_2-flux fractionation, exhibits the largest deviations from true depths. However, in the shallower UZ (above ~95 m), the scenarios that include Ar isotopes (1 and 2) display better agreement with true values than the scenarios that ignore Ar isotopes (3 and 4). We suggest that including Ar isotopes and neglecting CO_2-flux fractionation in future UZ applications (scenario 2) is justifiable for carefully selected sites with negligible deep CO_2 sources. However, for applications in sites where substantial deep sources of CO_2 in the past cannot be ruled out, the bias from excluding CO_2-flux fractionation would be significantly reduced by excluding Ar isotope measurements as inverse model constraints. Based the RMSD of scenarios 1 and 2, we suggest that the $\pm 1\sigma$ uncertainty of past water table depth estimation for carefully selected sites without strong CO_2 fluxes would be around 1 m, plus an additional contribution to total uncertainty from the conversion of dissolved gas to steady state UZ air isotope ratios.

5. Conclusions

Measured Ar, Kr, and Xe isotope profiles at ADRS are consistent with the hypothesis that steady state UZ fractionation is governed by gravitational settling, thermal diffusion, and diffusion against vertical fluxes of gases, after accounting for binary mixing with atmospheric air. Gravitational settling is the dominant fractionation process, leading to δ_i-depth profiles that are strongly dependent, nearly linear functions of depth for isotopes of these heavy noble gases. This is expected, as the magnitude of gravitational settling fractionation is independent of atomic mass (equation (4)) while the magnitudes of the water vapor and CO_2-flux fractionations decrease with atomic mass. By weighting isotope ratios by their sensitivity to gravitational settling, we demonstrate that an inverse model (section 2.4) can accurately estimate depth from a suite of high-precision Ar, Kr, and Xe isotope measurements.

The ability to estimate depth from UZ gas measurements has important applications for quantitative reconstructions of past climate change. Because dissolved gases in groundwater are inherited from the UZ air at the water table, we suggest that noble gas isotope measurements in paleogroundwater may enable accurate resolution of mean water table depth at the time of recharge. Laboratory determination of kinetic and solubility fractionation factors for noble gas isotope dissolution in water will be essential for this potential future application. With knowledge of past water table depth and geothermal gradient, NGTs may be used to reconstruct MAST with greater confidence by removing a bias associated with geothermal heat.

Together, accurate estimates of both water table depth and MAST may place important quantitative constraints helpful in understanding and modelling past hydroclimatic change.

Appendix A: Argon Isotope Correction

Due to erroneously low inlet pressures during the measurement of argon isotopes in the April 2015 samples, a small correction was made to the measured δ values. This correction was on average $-0.023‰$ and $-0.009‰$, and at most $-0.050‰$ and $-0.020‰$ for measurements of $\delta^{40}/_{36}$Ar and $\delta^{40}/_{38}$Ar, respectively. At low pressure, viscous flow of gas from the inlet to the source of the mass spectrometer begins to transition to molecular flow. This transition induces a small kinetic fractionation, such that the light isotope travels faster than the heavy one and is thus preferentially analyzed. At low Knudsen numbers (high pressure, low mean free path), this fractionation is negligible. However, because the April 2015 samples were analyzed at the end of a long sequence, there was insufficient gas remaining to reach a suitably high pressure. Although both sample and standard inlet pressures were lower than the set point of 5500 mV (expressed in terms of ^{36}Ar voltage), they were balanced. Despite approximately equal pressures between sample and standard gas, there was an apparent systematic trend among argon isotope measurement blocks of the same sample toward lower delta values with lower pressure. This trend was reproduced in subsequent lab experiments by intentionally varying the argon isotope measurement pressure from 3000 to 11,000 mV (~15–45 mbar) and examining the response in $\delta^{40}/_{36}$Ar and $\delta^{40}/_{38}$Ar. Because sample and standard inlet pressures were balanced, the mean free paths of argon molecules must have been similar. Thus, we hypothesize that at low pressures (high Knudsen numbers), small differences in the capillary diameters on the standard and sample sides of the inlet lead to differences in the degree of kinetic fractionation due to a reduction in viscous flow. Specifically, we suggest that a slightly narrower capillary on the standard side leads to more kinetic fractionation than the sample side at low total pressure. This would lead measured $\delta^{40}/_{36}$Ar and $\delta^{40}/_{38}$Ar to increase with a decrease in total pressure.

To remove this fractionation from our measurements, we determined apparent pressure sensitivities for $\delta^{40}/_{36}$Ar, $\delta^{40}/_{38}$Ar, and $\delta^{38}/_{36}$Ar from the 368 argon measurement blocks in the April 2015 data set. Apparent pressure sensitivity, *APS*, is defined as the slope of the geometric mean regression of measurement block delta anomalies, δ'_{block}, onto total pressure anomalies, V'_{36}.

$$APS = -\frac{\sigma\left(\delta'_{block}\right)}{\sigma\left(V'_{36}\right)} \tag{A1}$$

Block delta anomalies (in ‰) are defined as $\delta'_{block} = \delta_{block} - \overline{\delta}_{\text{sample}}$, where δ_{block} is the mean pressure imbalance-corrected delta value of a 16 cycle block and $\overline{\delta}_{\text{sample}}$ is the mean of δ_{block} among all measured aliquots of a given sample (typically four blocks/aliquot and six aliquots/sample). Pressure anomalies (in mV) are defined as $V'_{36} = V_{36,block} - 5500$ mV, where $V_{36,block}$ is the mean standard side intensity at mass 36 over the course of a block. Supporting information Figure S2 plots δ'_{block} against V'_{36} for all 368 argon isotope measurement blocks. The *APS* determined from these regressions are -0.00010, -0.00008, and $-0.00004‰$ mV^{-1} for $\delta^{40}/_{36}$Ar and $\delta^{40}/_{38}$Ar, respectively.

Original argon isotope δ_{block} measurements were then corrected using these *APS* values.

$$\delta_{block,corr} = \delta_{block} - V'_{36} \times APS \tag{A2}$$

For the deepest samples of each bore (108.8 m at UZB-2 and 103.9 m at UZB-3), two aliquots from each archived April 2015 sample were remeasured in May 2016 at higher argon pressure (11,000 mV). The mean correction among six UZB-2 108.8 m aliquots was rather small: $-0.006‰$ and $-0.002‰$ for $\delta^{40}/_{36}$Ar and $\delta^{40}/_{38}$Ar, respectively. However, the mean correction among six UZB-3 103.9 m aliquots was more substantial: $-0.049‰$ and $-0.020‰$ for $\delta^{40}/_{36}$Ar and $\delta^{40}/_{38}$Ar, respectively. The two sets of remeasured aliquots from each sample agreed well with the corrected values, as shown in supporting information Figure S3.

Appendix B: Prescribed Steady State CO_2 Profile

The CO_2 depth profile used in our steady state model was prescribed based on measurements compiled by *Walvoord et al.* [2005]. At ADRS, a persistent, deep CO_2 source is thought to govern steady state CO_2

concentrations, which increase with depth from atmospheric concentrations near the surface to as high as ~1% mole fraction at depth. Precipitation of calcite from groundwater supersaturated in bicarbonate and microbial activity in the saturated zone are the presumed sources of this deep CO_2 [*Walvoord et al*., 2005]. For our model, we use the measured UZB-2 CO_2 profile instead of UZB-3, because UZB-3 CO_2 concentrations are likely elevated between 0 and 60 m due to nonsteady state microbial source. High CO_2 concentrations at mid-UZ depths in UZB-3 (up to 2% mole fraction) coincide with high ^{14}C activity of CO_2 (up to 600,000% modern carbon), suggesting microbial respiration of a radioactive carbon source below the waste site [*Stonestrom et al*., 2004]. For our model, we approximated UZB-2 CO_2 as an exponential profile from 42 Pa at the surface to 960 ± 225 Pa at 108.8 m. The profile and its 1σ uncertainty are presented in supporting information Figure S4.

Appendix C: Agreement of Independent Versus Least Squares Contamination Estimates

Least squares estimates of atmospheric contamination (sections 2.4 and 3.2) are weighted by the measurement and model uncertainties of the eight isotope ratios used as constraints. Here we formally assess the degree to which estimates of atmospheric contamination inferred by individual isotope ratios agree with the least squares estimates. To start, we formally state our hypothesis of atmospheric contamination:

$$\delta_{meas} = (1 - f_{atm})\ \delta_{model} + f_{atm}\ \delta_{atm} \tag{C1}$$

where δ_{meas} and δ_{model} represent measurement and model isotope ratios, respectively, in a given sample. Noting that $\delta_{atm} = 0$ (by definition), we can rewrite (C1) and solve for f_{atm}.

$$f_{atm} = 1 - \frac{\delta_{meas}}{\delta_{model}} \tag{C2}$$

We can then rewrite an independent version of (C2) for any isotope ratio, *i*, with measurement and model means $\overline{\delta_{meas,i}}$ and $\overline{\delta_{model,i}}$, and uncertainties, $\delta'_{meas,i}$ and $\delta'_{model,i}$, respectively:

$$\overline{f_{atm,i}} \pm f'_{atm,i} = 1 - \frac{\overline{\delta_{meas,i}} \pm \delta'_{meas,i}}{\overline{\delta_{model,i}} \pm \delta'_{model,i}} \tag{C3}$$

We note that based on (C3) the individual atmospheric contaminant estimate uncertainties, $f'_{atm,i}$, are large for isotope ratios with high $\frac{\delta'_{meas,i}}{\delta_{meas,i}}$ and $\frac{\delta'_{model,i}}{\delta_{model,i}}$. For this reason, an unweighted average of all $\overline{f_{atm,i}}$ for *N* isotope ratio measurements (8 in our study) would not be a reasonable approach to estimate f_{atm}. Specifically, argon isotope ratios must be downweighted relative to other measured isotope ratios, because of their high model uncertainty. The heteroscedasticity of model and measurement uncertainties across the different isotope ratios is our justification for applying weighed least squares to estimate f_{atm} (section 2.4).

However, evaluating agreement between independent estimates $\overline{f_{atm,i}}$ and our least squares f_{atm} is a means to assess the validity of our atmospheric contamination hypothesis and subsequent correction. To carry out this evaluation, we estimate $\overline{f_{atm,i}}$ and $f'_{atm,i}$ via 1000 Monte Carlo simulations for each measured ratio *i* in each sample across both UZB-2 and UZB-3 (13 sample depths in total). We then compare the 95% confidence ranges of individual $f_{atm,i}$ estimates to the least squares estimate for each sample. Supporting information Figure S6 shows this comparison.

The 95% confidence intervals for all six krypton and xenon isotope ratios generally overlap with the least squares estimates. In roughly half of the sampled depths (6 of 13), argon isotope 95% confidence intervals do not agree with the least squares estimate. As discussed in the text, uncertainty about both horizontal thermal gradients and the background, steady state CO_2 profile limit our confidence in the applicability of the model for Ar isotopes at ADRS, given their high sensitivity to thermal diffusion and vertical gas fluxes.

We interpret "negative" atmospheric contaminant fractions inferred by Ar isotopes in the shallower UZ to be consistent with thermal diffusion fractionation in response to a waste-related heat source, which would cause Ar isotope ratios at UZB-2 and UZB-3 to be isotopically heavier. The good agreement of the atmospheric contaminant fractions estimated independently by the six Kr and Xe isotope ratios add confidence to the hypothesis of atmospheric contamination, since these isotope ratios are less sensitive to steady state gas fluxes and to thermal diffusion.

Acknowledgments

We thank the landowner State of Nevada, the site operator U.S. Ecology, and geologist Charles Feast for access to the site and assistance and advice with the field component of this study. USGS reviewer William C. Evans provided helpful feedback, as did three anonymous reviewers. Major funding was provided by the National Science Foundation's Graduate Research Fellowship Program and through NSF grant OPP05-21642. USGS funding was provided through the Toxic Substances Hydrology Program and the National Research Program. All individual aliquot measurements of Ar, Kr, and Xe isotope ratios during campaigns A and B are included in the supporting information. Trade names are used for identification purposes only and do not imply product endorsement.

References

Aeschbach-Hertig, W., and D. K. Solomon (2013), Noble gas thermometry in groundwater hydrology, in *The Noble Gases as Geochemical Tracers*, edited by P. Burnard, pp. 81–122, Springer, Berlin, Heidelberg.

Aeschbach-Hertig, W., F. Peeters, U. Beyerle, and R. Kipfer (2000), Palaeotemperature reconstruction from noble gases in ground water taking into account equilibration with entrapped air, *Nature*, *405*(6790), 1040–1044, doi:10.1038/35016542.

Andraski, B. J. (1996), Properties and variability of soil and trench fill at an arid waste-burial site, *Soil Sci. Soc. Am. J.*, *60*(1), 54–66.

Baker, R. J., B. J. Andraski, D. A. Stonestrom, and W. Luo (2012), Volatile organic compounds in the unsaturated zone from radioactive wastes, *J. Environ. Qual.*, *41*(4), 1324–1336, doi:10.2134/jeq2011.0480.

Craig, H., Y. Horibe, and T. Sowers (1988), Gravitational separation of gases and isotopes in polar ice caps., *Science*, *242*(4886), 1675–1678, doi:10.1126/science.242.4886.1675.

Ding, X., B. M. Kennedy, W. C. Evans, and D. A. Stonestrom (2016), Experimental studies and model analysis of noble gas fractionation in porous media, *Vadose Zone J.*, *15*(2), 12, doi:10.2136/vzj2015.06.0095.

Freundt, F., T. Schneider, and W. Aeschbach-Hertig (2013), Response of noble gas partial pressures in soil air to oxygen depletion, *Chem. Geol.*, *339*, 283–290, doi:10.1016/j.chemgeo.2012.07.026.

Fuller, E. N., P. D. Schettler, and J. C. Giddings (1966), A new method for prediction of binary gas-phase diffusion coefficients, *Ind. Eng. Chem.*, *16*(10), 551, doi:10.1016/0042-207X(66)90400-3.

Grachev, A. M., and J. P. Severinghaus (2003), Determining the thermal diffusion factor for $^{40}Ar/^{36}Ar$ in air to aid paleoreconstruction of abrupt climate change, *J. Phys. Chem. A*, *107*(23), 4636–4642, doi:10.1021/jp027817u.

Green, C. T., M. A. Walvoord, B. J. Andraski, R. G. Striegl, and D. A. Stonestrom (2015), Multimodel analysis of anisotropic diffusive tracer-gas transport in a deep arid unsaturated zone, *Water Resour. Res.*, *51*, 6052–6073, doi:10.1002/2014WR016055.

Grew, K., and T. Ibbs (1953), Thermal diffusion in gases, *Q. J. R. Meteorol. Soc.*, *79*(341), 458–458, doi:10.1002/qj.49707934127.

Guillon, S., C. Gréau, and E. Pili (2016), Continuous monitoring of the vadose zone gas phase by mass spectrometry, *Vadose Zone J.*, *15*(8), 6, doi:10.2136/vzj2015.12.0168.

Hamme, R. C., and J. P. Severinghaus (2007), Trace gas disequilibria during deep-water formation, *Deep Sea Res., Part I*, *54*(6), 939–950, doi:10.1016/j.dsr.2007.03.008.

Johnson, M. J., C. J. Mayers, and B. J. Andraski (2002), Selected micrometeorological and soil-moisture data at Amargosa Desert Research Site in Nye County near Beatty, Nevada, 1998–2000, *U.S. Geol. Surv. Open File Rep., 2002-348*, 29.

Johnson, M. J., C. J. Mayers, and B. J. Andraski (2007), Selected micrometeorological, soil-moisture, and evapotranspiration data at Amargosa Desert Research Site in Nye County near Beatty, Nevada, 2001–05, *U.S. Geol. Surv. Data Ser., 284*, 38.

Kawamura, K., J. P. Severinghaus, M. R. Albert, Z. R. Courville, M. A. Fahnestock, T. Scambos, E. Shields, and C. A. Shuman (2013), Kinetic fractionation of gases by deep air convection in polar firn, *Atmos. Chem. Phys.*, *13*(21), 11,141–11,155, doi:10.5194/acp-13-11141-2013.

Kipfer, R., W. Aeschbach-Hertig, F. Peeters, and M. Stute (2002), Noble gases in lakes and ground waters, *Rev. Mineral. Geochem.*, *47*(1), 615–700, doi:10.2138/rmg.2002.47.14.

Mayers, C. J., B. J. Andraski, C. A. Cooper, S. W. Wheatcraft, D. A. Stonestrom, and R. L. Michel (2005), Modeling tritium transport through a deep unsaturated zone in an arid environment, *Vadose Zone J.*, *4*(4), 967–976, doi:10.2136/vzj2004.0179.

Mazor, E. (1972), Paleotemperatures and other hydrological parameters deduced from noble gases dissolved in groundwaters; Jordan Rift Valley, Israel, *Geochim. Cosmochim. Acta*, *36*(12), 1321–1336, doi:10.1016/0016-7037(72)90065-8.

Mourzenko, V. V., C. Varloteaux, S. Guillon, J.-F. Thovert, E. Pili, and P. M. Adler (2014), Barometric pumping of a fractured porous medium, *Geophys. Res. Lett.*, *41*, 6698–6704, doi:10.1002/2014GL060865.

Phillips, F. M. M. (1981), Noble gases in ground water as paleoclimatic indicators, PhD. thesis, Univ. of Ariz., Tucson, Arizona.

Reid, R. C., J. M. Prausnitz, and T. K. Sherwood (1977), *The Properties of Gases And Liquids*, 3rd ed., 688 pp., McGraw-Hill, New York.

Severinghaus, J. P., and M. O. Battle (2006), Fractionation of gases in polar ice during bubble close-off: New constraints from firn air Ne, Kr and Xe observations, *Earth Planet. Sci. Lett.*, *244*(1–2), 474–500, doi:10.1016/j.epsl.2006.01.032.

Severinghaus, J. P., M. L. Bender, R. F. Keeling, and W. S. Broecker (1996), Fractionation of soil gases by diffusion of water vapor, gravitational settling, and thermal diffusion, *Geochim. Cosmochim. Acta*, *60*(6), 1005–1018, doi:10.1016/0016-7037(96)00011-7.

Severinghaus, J. P., T. Sowers, E. J. Brook, R. B. Alley, and M. L. Bender (1998), Timing of abrupt climate change at the end of the Younger Dryas 8 interval from thermally fractionated gases in polar ice, *Nature*, *391*(6663), 141–146, doi:10.1038/34346.

Severinghaus, J. P., A. Grachev, and M. Battle (2001), Thermal fractionation of air in polar firn by seasonal temperature gradients, *Geochem. Geophys. Geosyst.*, *2*(7), 1048, doi:10.1029/2000GC000146.

Stanley, R., and W. Jenkins (2013), Noble gases in seawater as tracers for physical and biogeochemical ocean processes, in *The Noble Gases as Geochemical Tracers*, edited by P. Burnard, pp. 55–79, Springer, Berlin, Heidelberg, doi:10.1007/978-3-642-28836-4.

Stonestrom, D., J. Abraham, B. Andraski, R. Baker, C. Mayers, R. Michel, D. Prudic, R. Striegl, and M. Walvoord (2004), Monitoring radionuclide contamination in the unsaturated zone: Lessons learned at the Amargosa Desert Research Site, Nye County, Nevada, in *Workshop on Long-Term Performance Monitoring of Metals and Radionuclides in the Subsurface, Reston, VA*, pp. 21–22, United States Geological Survey, Reston, Va.

Stute, M., and P. Schlosser (1993), Principles and applications of the noble gas paleothermometer, in *Climate Change in Continental Isotopic Records*, edited by P. K. Swart, K. C. Lohmann, J. Mckenzie and S. Savin, American Geophysical Union, Washington, D. C., doi:10.1029/GM078p0089.

Stute, M., M. Forster, H. Frischkorn, A. Serejo, J. F. Clark, P. Schlosser, W. S. Broecker, and G. Bonani (1995), Cooling of tropical Brazil (5°C) during the Last Glacial Maximum, *Science*, *269*(5222), 379–383, doi:10.1126/science.269.5222.379.

Tempest, K. E., and S. Emerson (2013), Kinetic isotopic fractionation of argon and neon during air-water gas transfer, *Mar. Chem.*, *153*, 39–47, doi:10.1016/j.marchem.2013.04.002.

Tomonaga, Y., R. Blättler, M. S. Brennwald, and R. Kipfer (2012), Interpreting noble gas concentrations as proxies for salinity and temperature in the world's largest soda lake (Lake Van, Turkey), *J. Asian Earth Sci.*, *59*, 99–107, doi:10.1016/j.jseaes.2012.05.011.

Tyroller, L., M. S. Brennwald, L. Mächler, D. M. Livingstone, and R. Kipfer (2014), Fractionation of Ne and Ar isotopes by molecular diffusion in water, *Geochim. Cosmochim. Acta*, *136*, 60–66, doi:10.1016/j.gca.2014.03.040.

Walvoord, M. A., D. A. Stonestrom, B. J. Andraski, and R. G. Striegl (2004), Constraining the inferred paleohydrologic evolution of a deep unsaturated zone in the Amargosa Desert, *Vadose Zone J.*, *3*(2), 502–512, doi:10.2136/vzj2004.0502.

Walvoord, M. A., R. G. Striegl, D. E. Prudic, and D. A. Stonestrom (2005), CO_2 dynamics in the Amargosa Desert: Fluxes and isotopic speciation in a deep unsaturated zone, *Water Resour. Res.*, *41*, W02006, doi:10.1029/2004WR003599.

Weeks, E. P., D. E. Earp, and G. M. Thompson (1982), Use of atmospheric fluorocarbons F11 and F12 to determine the diffusion parameters of the unsaturated zone in the Southern High Plains of Texas, *Water Resour. Res.*, *18*(5), 1365–1378, doi:10.1029/WR018i005p01365.

Weisbrod, N., M. I. Dragila, U. Nachshon, and M. Pillersdorf (2009), Falling through the cracks: The role of fractures in Earth-atmosphere gas exchange, *Geophys. Res. Lett.*, *36*, L02401, doi:10.1029/2008GL036096.